Journal of Engineering Science and Technology
Vol. 15, No. 2 (2020) 1319 - 1337

ADAPTIVE WINDOW- BASED FRACTAL DIMENSION ESTIMATION FOR WEIGHT MAPS IN CONTRAST IMPROVED MULTI- SENSOR FUSION

T. SANDHYA KUMARI[1,*], S. KOTESWARA RAO[2], I. SANTI PRABHA[3]

[1]Department of Electronics & Communication Engineering, Vignan's Institute of Engineering for women, Visakhapatnam, Andhra Pradesh, India
[2]Department of Electronics & Communication Engineering, K.L.University, Vaddeswaram, Guntur District, Andhra Pradesh, India
[3]Department of Electronics & Communication Engineering, J.N.T. University, Kakinada,Andhra pradesh, India
*Corresponding Author: teku.sandhya@gmail.com

Abstract

In this paper, as a primary processing step, visible images acquired at low illumination conditions are processed. Lower and large parameter based Stochastic Resonance models in Discrete Wavelet Transform domain is considered for primary processing. The pre-processing approach prior to fusion provides better scene interpretation and improves the performance of visible sensor sensitivity to night or low dynamic conditions. The contrast-enhanced visible image and infrared image fusion are then performed using a weighted average scheme. In the proposed algorithm, the weights considered for fusion are calculated using an adaptive window-based Fractal Dimension computation. Adaptive window-based Fractal Dimension weight maps computed in this approach has a significant effect on improving the sharpness and edge information of the final fused image. The quantitative features of the fused image in terms of its contrast, sharpness, symmetry and visual information are evaluated. Simulation results on various test images prove that the proposed approach for fusion is simple and has enhanced quality and quantitative outcome compared to recent techniques.

Keywords: Adaptive window, Contrast enhancement, Fractal dimension, Multi-Sensor fusion.

1. Introduction

Acquiring complete information from a single sensor is incomplete because of sensor capability limitations. Images captured by multiple sensors provide complementary information of the same scene. Image fusion, the technique of combining corresponding information captured by multiple sensors to a single image intensifies the comprehensive understanding of the scene. Multi-sensor image fusion allows the human to interpret the situation without being hindered by eye strain and find a wide range of usage in night vision, surveillance, military, defence, security and civilian applications [1-3].

Night vision devices, multi-sensor systems and fused imagers that provide excellent human observing capabilities for target detection, scene interpretation and monitoring employ infrared and visible sensor fusion. Images captured by visible sensor provide texture details and infrared sensor provides target details. Image information from multiple sensors can be combined directly in the spatial domain through an appropriate fusion rule such as select maximum, weighted average, Principle Component Analysis [4] and Spatial Frequency [5] based fusion techniques. The spatial domain-based fusion techniques were computationally simple, efficient and are used for several real-time applications. However, processing the images directly in the spatial domain causes contrast reduction and missing of some details in the final image. These limitations are conquered by multi-scale fusion techniques where the images are first decomposed to different scales and the coefficients are combined by a specific fusion rule. Finally, the image is reconstructed by applying the inverse multi- scale transform to the fused coefficients. Laplacian Pyramid (LP) [6], Contrast Pyramid Transform(CP) [7],

Discrete Wavelet Transform (DWT) [8], Wavelet Structured Discrete Cosine Transform (WSDCT) [9], Guided Filtering (GF) [10], Karhunen-Loeve Transform [11], and Singular Value Decomposition (SVD) [12] etc., are some of the multi-scale techniques in literature employed for fusion. Though, these techniques provide detail preservation, texture information and improved contrast in the fused image, computational time and selection of a proper transform for multi-scale decomposition are few drawbacks that limits these methods for real-time implementation. Therefore, investigation on multi-sensor fusion by an effective spatial domain technique is still a continuing research. Recently, local activity [13] based fusion for infrared and a visible image, local binary pattern based weight map construction in spatial domain [14] has gained attention to researchers to continue their research for multi-sensor fusion in spatial domain.

However, the fusion technique for infrared and visible sensor fusion in literature [15] concentrates on the fusion methodologies and fusion rules. But, the sensor sensitivity to poor lighting conditions and weather changes are few challenges that affect the accuracy and efficiency of the fused image. The performance of a visible sensor is affected by its low sensitivity to dark nights and low dynamic range to bright days that results in poor contrast or dark images. Hence, in the proposed approach, the primary focus is to improve the quality of the images captured by visible sensors under low lighting conditions. Stochastic Resonance (SR) based enhancement approach in spatial and transform domains to low-light or dark images [16-18] has showed outstanding performance compared to traditional [19] and several non SR methods [20-22].

Selection of parameters and metrics in SR plays a key role in reducing the oversaturation and noise in the output image. Parameters are derived by maximizing signal to noise ratio [23], entropy [24], or minimizing noise [25] in traditional dynamic SR system excited by weak noise and low frequency signals. In [26], the low frequency signals are handled by smaller parameters and high-frequency signals by larger parameters in order to extract the features of both low and high-frequency components effectively. Considering the same scenario to an image, in this work, a smaller parameter based SR model is used to tune the low frequency coefficients while a larger parameter based SR model is used to tune the high-frequency coefficients of DWT to achieve improved contrast change in low light visible image.

Fractal Dimension (FD) is a powerful metric in image processing for texture classification and edge detection. Local Fractal Dimension (LFD) measures the local surface roughness [27] and also distinguishes the noise component from the edge component [28]. Recently, LFD features of multiple source images are extracted and are utilized in the multi-sensor fusion [29]. The window size selected for computing LFD varies depending on edge or smooth surface in an image [30]. Therefore, adaptive window-based FD estimation for weighted average fusion of contrast improved multi-sensor images is proposed in this paper. The visible sensor sensitivity to low light conditions or dark nights is improved by small and large parameter based SR model. Thus, the traditional SR model using the same parameters to tune both the low and high frequency coefficients may not produce the desirable contrast or may lead to oversaturation. Hence, in this paper, the parameters for high frequency coefficient tuning are selected to be '*m*' times the values selected for low frequency coefficients, where '*m*' is large. Further, adaptive window-based FD maps of improved visible and infrared images are computed for weighted average fusion. The advantages of the proposed method are it is computationally efficient, simple spatial domain fusion technique that improves the contrast, increases the sharpness and edge information of the final fused image without any loss of information from the two source images.

The proposed fusion framework is explained in Section 2. Simulations on various test images demonstrate the enhanced quality and quantitative outcome. The quantitative and qualitative evaluation, results and discussion of the proposed work is elaborated in Sections 3 and 4. Conclusions and future work is addressed in Section 5.

2. Proposed Fusion Method

The proposed fusion framework performs three steps to complete the fusion task:

(a) Contrast improvement of low-light visible image DWT coefficients by lower and higher parameter based SR model.
(b) Adaptive window-based FD calculation to construct fractal maps.
(c) Construct weight maps for fusion.

The structure of the proposed work is shown in Fig. 1 and the description of each process in detail is given in the ensuing sections. As the algorithmic steps are implemented directly in spatial domain, the algorithm is computationally efficient and it increases the sharpness and edge information in the final fused image.

2.1. Contrast improvement of low-light visible image DWT coefficients by lower and higher parameter based SR model

The sensitivity of the visible sensor to poor lighting conditions reduces the contrast of the image and so the information is not clear to human vision. Hence, to increase the quality of such an image, it is required to process it for further operations. Decomposition based enhancement techniques are found to be more efficient in contrast improvement compared to several traditional spatial domain techniques [31, 32]. Good localization, directionality and perfect reconstruction properties of DWT made the transform more popular in image processing tasks. DWT measures intensity changes of an image along horizontal, vertical and diagonal directions that indicate the edge details along these directions [19].

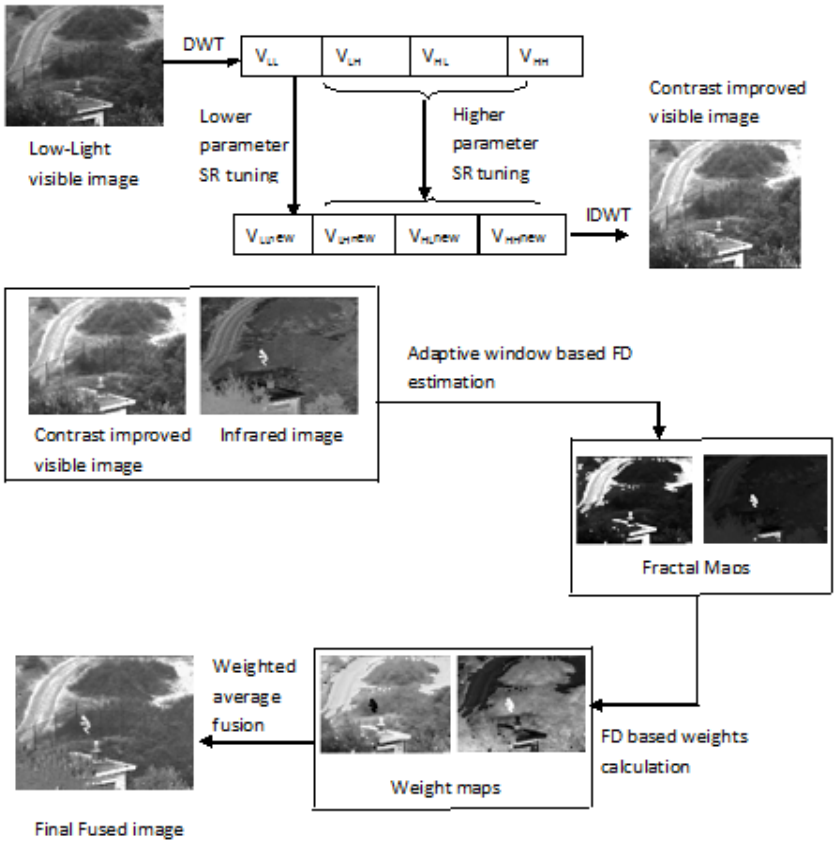

Fig. 1. Entire structure of the proposed work.

Let '*V*' be the image captured by a visible sensor at low or dark night conditions. Applying DWT to '*V*' decomposes it into low and high-frequency coefficients as V_{LL}, V_{LH}, V_{HL} and V_{HH}respectively. The low frequency coefficients are tuned by a lower SR modelled as:

$$V_{LLnew}(n+1) = V_{LLnew}(n) + \Delta t[a_l V_{LLnew}(n) - b_l V_{LLnew}^3(n) + V_{LL}] \quad (1)$$

Equation (1) is the traditional SR model applicable for low-frequency signal and the parameters $a_l<1$, $b_l<1$ are smaller parameters of SR. An optimum value of 'a_l' is defined [33] to be $a_1 = 2\sigma_0^2$, with σ_0^2 as the variance of the input V_{LL}.$\Delta t$is the sampling interval that determines the tuning range and $V_{LLnew}(0) = 0$. The condition required by the parameter 'b_l' is given by$b_1 \leq \frac{4a^3}{27}$

For high-frequency coefficients, the SR is modelled with 'a_h' and 'b_h' as higher parameters of SR as:

$$V_{LHnew}(n+1) = V_{LHnew}(n) + \Delta t[a_h V_{LHnew}(n) - b_h V_{LHnew}^3(n) + V_{LH}] \quad (2)$$

$$V_{HLnew}(n+1) = V_{HLnew}(n) + \Delta t[a_h V_{HLnew}(n) - b_h V_{HLnew}^3(n) + V_{HL}] \quad (3)$$

$$V_{HHnew}(n+1) = V_{HHnew}(n) + \Delta t[a_h V_{HHnew}(n) - b_h V_{HHnew}^3(n) + V_{HH}] \quad (4)$$

The smaller and larger parameters are related by $a_l=a_h/m$ and $b_l=b_h/m$, where 'm' is a scaling factor that needs to be appropriately selected to produce optimal SR response. Experimentally, after several simulations on various test images, the value of $m=1000$, 'Δt' = 0.0015 are selectedin this work. Initially, $V_{LHnew}(0) = 0$, $V_{HLnew}(0) = 0$, $V_{HHnew}(0) = 0$are assumed. The number of iterations to achieve the resonance state is indicated by 'n'. Entropy, a measure of contrast is used as a metric for terminating the iterations, once the value starts decreasing. The tuned coefficients are reconstructed by applying Inverse Discrete Wavelet Transform to get the contrast improved visible image 'V_1'.

Low light visible RGB image retrieved from [34] is considered to demonstrate the performance of low and high parameter based SR model in Fig. 2.

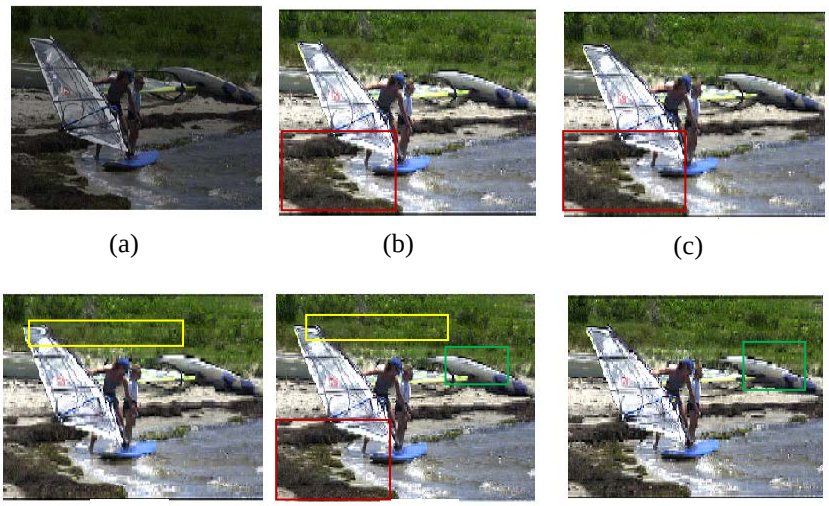

(a) (b) (c)

(d) (e) (f)

Fig. 2. (a) Low-light Visible image (b) contrast enhanced image with m=1(Classical SR), (c) m=10, (d) m=100, (e) m=1000, and (f) m=2000.

The input low light visible image is shown in Fig. 2(a) and the experimental results for different values of 'm' are shown in Fig. 2 (b)-Fig. 2(f) respectively. Comparison of the results for m=1000 to other values of 'm' shows that the contrast

is less for lower values of m=1 *(classical SR)* and m=10 as highlighted by rectangles with *'red'* colour. Higher value of '*m'* over sharpens the image indicated by rectangle with *'green'* and for m=100, it is observed that the image gets blurred in certain regions of contrast as indicated by rectangle with *'yellow'* colour. Hence, the selection of '*m'* in the proposed model has a significant effect in controlling the over saturation and over sharpening effects in addition to contrast improvement.

2.2. Adaptive window-based FD calculation to construct Fractal maps

The FD based image processing applications such as texture analysis, classification [35], edge detection [36], and segmentation [37], etc. relies on accurate FD measurement. The three basic components of an image are edges, texture and smooth areas. FD is a measure that describes the roughness of an image. LFD is a descriptor of local surface roughness. The computational simplicity of Blanket method made it a popular technique for computing FD. The mathematical steps to compute LFD value using Blanket method is briefly given as follows:

Step 1: The upper 'u_r' and lower 'l_r' surfaces of an image pixel $I(i, j)$ located at (i, j) is computed as:

$$u_r = max\{u_{r-1}(i,j) + 1, max_{|(p,q)-(i,j)|\leq 1} u_{r-1}(p,q)\} \tag{5}$$

$$l_r = min\{l_{r-1}(i,j) + 1, min_{|(p,q)-(i,j)|\leq 1} l_{r-1}(p,q)\} \tag{6}$$

where (p, q) and (i, j) are the pixel locations located at a distance less than 1,' r' represents number of blankets and $u_0(i,j)=l_0(i,j)=I(i,j)$.

Step 2: The blanket area is then computed as:

$$A(r) = \frac{\sum_{i,j} u_r(i,j) - l_r(i,j)}{2r} \tag{7}$$

Step 3: The LFD value is then estimated from the surface area given by:

$$A(r) = \frac{wK}{D} r^{2-D} \tag{8}$$

where 'W' is the window size, 'K' is a Constant and 'D' is the LFD of the surface. The estimated LFD for a fixed window size is low for a smooth surface and is high for rough surface. Fixed window based LFD estimation will affect the detection of edges because LFD varies significantly with the window size in the edge regions. Taking into consideration, the variation of LFD value with window size, an adaptive window to extract the smooth, rough and edge region features is proposed.

Let $w = 5$ be the initial window size centred on a pixel $I(i, j)$ located at (i, j). The Blanket method is used for computing the LFD value *'D'*. Based on the conditions that for smooth regions, the LFD value is low and approaches a value close to 2, for rough regions, the value is high and is close to 3, the window in our proposed method is made adaptive as shown in Fig. 3. Once an appropriate window is selected, the LFD value for the selected window size is computed at pixel (i, j). This process is repeated for all the pixels in the entire image to determine the fractal map 'FM' of an image. In the context of the proposed fusion process, if 'V_1' and 'I_1' are the enhanced visible and infrared images then the fractal maps 'FM_1' and 'FM_2' are constructed using this adaptive window-based FD estimation.

$$W = \begin{cases} 5; & D < 2 \\ 3; & 2 < D < 3 \\ 7; & D > 3 \end{cases}$$

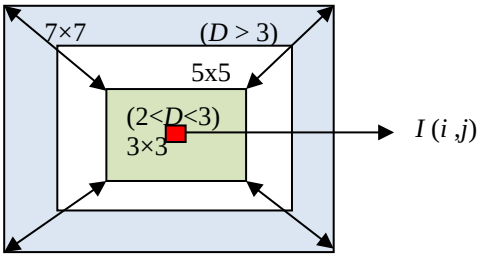

Fig. 3. Mathematical representation and illustration of adaptive window.

2.3. Construct weight maps for fusion

Weighted average fusion is one of the fundamental fusion rule employed in multi-sensor fusion process. In weighted average fusion, the weights are selected such that the sum of these weights should not exceed unity. Weights for fusion were selected based on several statistical characteristics such as standard deviation, entropy, spatial frequency, etc. in literature [38]. In the proposed work, the weights for fusions are selected based on the texture, smooth and edge characteristics described by FD. The weight maps 'WM_1' and 'WM_2' are computed by taking the average of fractal maps obtained for contrast improved visible and infrared images as:

$$WM_1 = \frac{FM_1 + FM_2}{2} \tag{9}$$

$$WM_2 = 1 - WM_1 \tag{10}$$

such that $WM_1 + WM_2 = 1$. Once the weight maps are constructed then the final fused image 'FF' is obtained as:

$$FF = WM_1 * V_1 + WM_2 * I_1 \tag{11}$$

The enhancement of visible image prior to fusion in the proposed method provides better visual quality for efficient scene interpretation. The adaptive window-based FD estimation considers the description of smooth, texture and edge regions of the image. The weighted average fusion based on FD in the spatial domain simplifies the technique.

3. Evaluation of the Proposed Method

The algorithms proposed for multi-sensor fusion should meet the requirements that the final fused image contains the essential complementary information available in the source images without any loss of details and artefacts. The information should be clear for human interpretation and the methodology is simple and reliable. Evaluation of the fusion algorithm is done qualitatively by visual judgment made by some human observers. However, qualitative evaluation is based on the rating given by the observers and may not be accurate. Hence, quantitative evaluation metrics define the accuracy, reliability and robustness of the algorithm. Quantitative evaluation metrics considered for the proposed algorithm are Mean Pixel Intensity (MPI) and Standard Deviation (SD) that describes the contrast, Entropy (E) and Fusion Symmetry (FS) that describes the information content, Spatial Frequency (SF) and Visible Information Fidelity (VIF) that gives the visual

quality and Average Gradient (AG) that describes the edge information of the final fused image. The metrics are briefly discussed as:

1) Mean Pixel Intensity (MPI): An index that describes the contrast of an image is the Mean Pixel Intensity (MPI) given by:

$$MPI = \frac{1}{MN}\sum_{i=1}^{M}\sum_{j=1}^{N} I(i,j) \tag{12}$$

where *MN* is the size of the image and *I (i, j)* is the pixel intensity of image *I* at location *(i, j).*

Standard Deviation (SD): Another contrast evaluation metric of an image is Standard Deviation (SD) where high value of SD indicates high contrast of the image defined as:

$$SD = \sqrt{\frac{\sum_{i=1}^{M}\sum_{j=1}^{N}[I(i,j) - MPI]^2}{MN}} \tag{13}$$

2) Entropy (E): Maximum information content in an image is measured by Entropy defined as:

$$E = \sum_{i=1}^{M}\sum_{j=1}^{N} p(I_{i,j}) \ln p(I_{i,j}) \tag{14}$$

where $p(I_{i,j})$ is the probability of occurrence of the pixel at (i, j).

3) Fusion Symmetry (FS): Symmetry of the final fused image with respect to the source images is measured by the metric Fusion Symmetry (FS). The low the value of FS, the better is the algorithm and more symmetric is the final fused image. FS is defined as:

$$FS = abs(\frac{MI_{AF}}{MI_{AF} + MI_{BF}} - 0.5) \tag{15}$$

where MI_{AF} and MI_{BF} is the mutual information shared between the source images A, B and Fused image F expressed as:

$$MI_{AF} = \sum_{a,b} p_{AF}(a,b) log \frac{p_{AF}(a,b)}{p_A(a,b)p_F(a,b)} \tag{16}$$

$$MI_{BF} = \sum_{a,b} p_{BF}(a,b) log \frac{p_{BF}(a,b)}{p_B(a,b)p_F(a,b)} \tag{17}$$

where $P_{AF}$and $P_{BF}$are the joint probabilities and P_A, P_B and P_F are the marginal probabilities.

4) Average Gradient (AG): The clarity and sharpness of the final fused image is described by the edge-based metric AG defined as:

$$AG = \frac{1}{MN}\sum_{i=1}^{M}\sum_{j=1}^{N}\sqrt{\frac{[I(i+1,j)-I(i,j)]^2+[I(i,j+1)-I(i,j)]^2}{2}} \quad (18)$$

5) Spatial Frequency (SF): The global activity level of the final fused image is described by SF. Higher the value of the SF, better is the visual quality of the image expressed mathematically as:

$$SF = \sqrt{\frac{1}{MN}\left[\sum_{i=1}^{M}\sum_{j=2}^{N}(I(i,j)-I(i,j-1))^2+\sum_{j=1}^{N}\sum_{i=2}^{M}(I(i,j)-I(i,j-1))^2\right]} \quad (19)$$

6) Visible Information Fidelity (VIF): Human visual perception based metric for evaluating the visual quality of the image is VIF computed using the algorithmic steps proposed earlier [39]. The higher the value better is the visual quality.

4. Results and Discussions

Images acquired by visible and infrared sensors used in military, weapon detection, surveillance and civilian applications are taken for simulation in MATLAB. Gray scale image data set available at [40, 41] are considered for experimental evaluation as shown in Fig. 4.

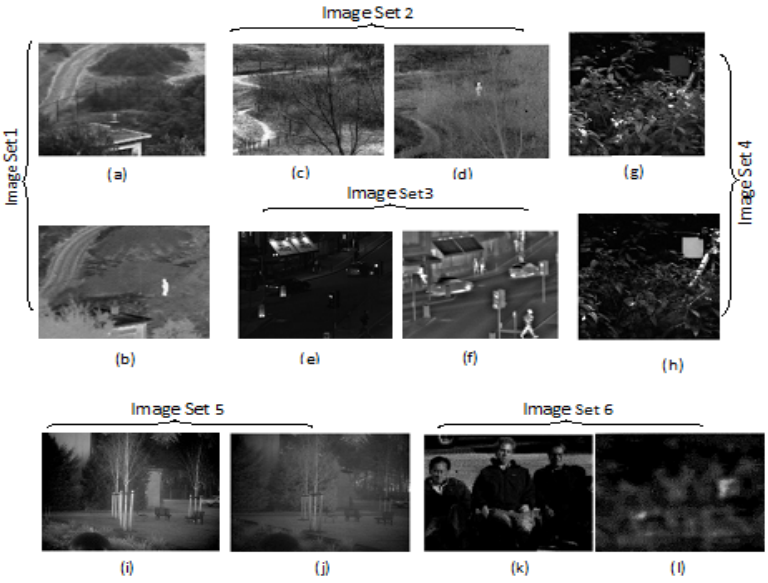

.

Fig. 4. Image data sets 1-6.

Directive Contrast in DWT (DCDWT) [42], Anisotropic Diffusion (AD) [11], PCADWT [43] and FD [29] based fusion methods in literature. Fusion results of image set 1 & set 2 are used in military applications for target detection. Fig. 5(a) is the result of LP method that could not preserve all the details of the source images. Figures 5(b) and 5(c) are the results of CP and GF that introduce artifacts in the output image. Figures 5(d), 5(e) and 5(f) are the results obtained for

WSDCT, DCDWT and AD methods that suffers from poor contrast and are blurred. Figure 5(g) is the result of PCADWT that makes the grass region of the image darker and results in poor human visual perception. Figure 5(h) is the result of FD method that has good contrast compared to the other methods. However, the proposed method result shown in Fig. 5(i) improves the overall contrast of the image providing all the information from the sources for easy interpretation of the scene. The edge details of the target are preserved in Fig 5 (i) as a result of extracting the edge features in addition to smooth and rough regions using adaptive window-based FD estimation.

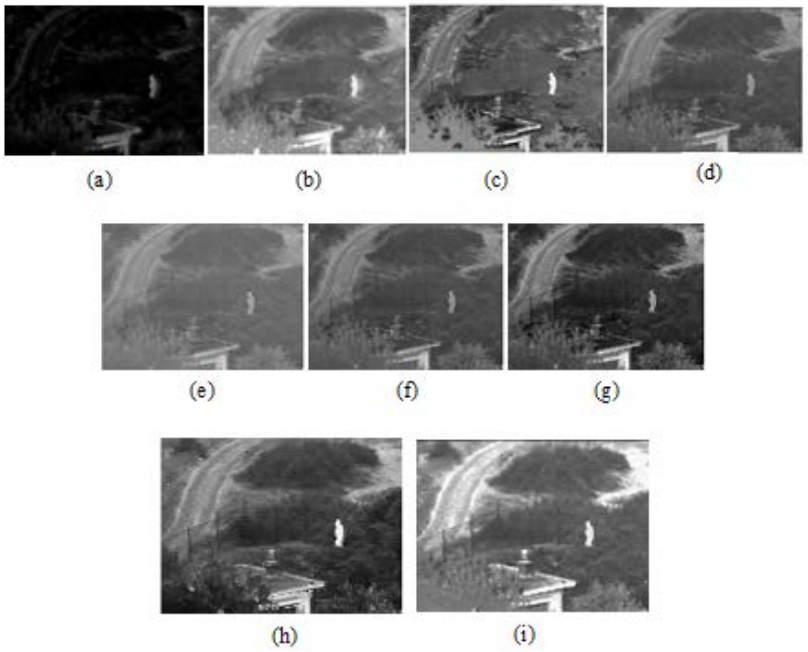

Fig. 5. Comparison of qualitative results of data set Image 1 (a) LP [6], (b) CP [7], (c) GF [10], (d) WSDCT [9], (e) DCDWT [42], (f) AD [11], (g) PCADWT [43], (h) FD [29], (i) Proposed.

Simulation results of data set image 2 are shown in Fig. 6. The results obtained by GF, AD and FD methods are visually better but the edge symmetry is missing in Fig. 6(h), the target details are missing in Fig. 6(g) and the details on the far end of the target region are not clear in Fig. 6(c). The proposed method result in Fig. 6(i) shows significant contrast improvement over the entire image. The target details are clear with structural preservation of the person behind the tree. Data set image 3 is for surveillance application. The results obtained by the proposed method shown in Fig. 7(i) gives the complete information of the scene captured when compared to the other existing techniques. Poor contrast and missing of thestructure and texture details are observed in Fig. 7(c) - Fig. 7(h). Though the details are clear, blurring is observed in Fig. 7(b) and Fig. 7(a) respectively. The simulation results of data set images 4 and 5 shown in Figs. 8 and 9 prove that the proposed method is best suited for civilian applications. High contrast, no loss of

information and better visual perception is achieved as shown in Fig. 8(i) and Fig. 9(i) respectively.

Table 1. Quantitative metrics of data set Image 1.

Method / Metric	*MPI*	*SD*	*E*	*FS*	*AG*	*SF*	*VIF*
LP	13.144	16.195	5.164	0.028	1.821	3.727	0.105
CP	118.95	31.03	6.724	0.019	2.583	5.219	0.288
GF	98.314	28.826	6.768	**0.005**	6.166	11.974	0.196
WSDCT	89.952	22.683	6.255	0.017	4.998	9.282	0.311
DCDWT	88.913	24.372	6.363	0.014	5.226	11.776	0.247
AD	90.015	22.517	6.239	0.019	4.267	7.781	0.312
PCADWT	90.081	22.392	6.228	0.017	3.774	7.042	0.313
FD	84.604	40.267	**7.164**	0.08	5.406	13.146	0.250
Proposed	**122.54**	**43.526**	7.019	0.015	**15.756**	**14.015**	**0.341**

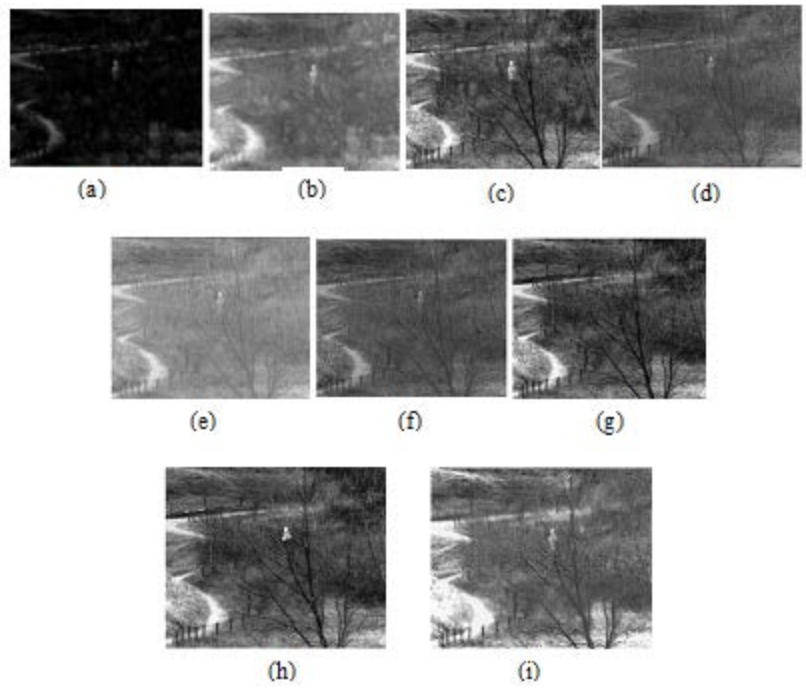

Fig. 6. Comparison of qualitative results of data set Image 2 (a) LP [6], (b) CP [7], (c) GF [10], (d) WSDCT [9], (e) DCDWT [42], (f) AD [11], (g) PCADWT [43], (h) FD [29], (i) Proposed.

Data set image 6 for weapon detection application is takenfor simulation and results are shown in Fig. 10. It is observed that the background details, target details and the structure information are clear in the proposed work compared to other methods considered for comparison. Hence, the qualitative results of all the data set images shows that the proposed method clearly shows the details of both the source images amassed in the final fused image.

Table 2. Quantitative metrics of data set Image 2.

Method / Metric	*MPI*	*SD*	*E*	*FS*	*AG*	*SF*	*VIF*
LP	14.602	14.341	5.277	0.058	2.058	3.895	0.112
CP	116.672	30.88	6.662	0.044	2.833	5.149	0.205
GF	90.158	38.931	7.095	0.067	9.751	16.788	**0.272**
WSDCT	86.077	19.128	6.155	0.05	8.405	14.155	0.245
DCDWT	84.833	20.258	6.198	0.047	6.317	11.554	0.161
AD	86.137	18.781	6.117	0.05	6.804	11.328	0.252
PCADWT	86.695	35.554	6.957	0.048	8.815	15.027	0.215
FD	87.830	40.348	**7.164**	0.073	10.278	18.145	0.243
Proposed	**117.859**	**43.368**	6.985	**0.042**	**11.535**	**22.484**	0.234

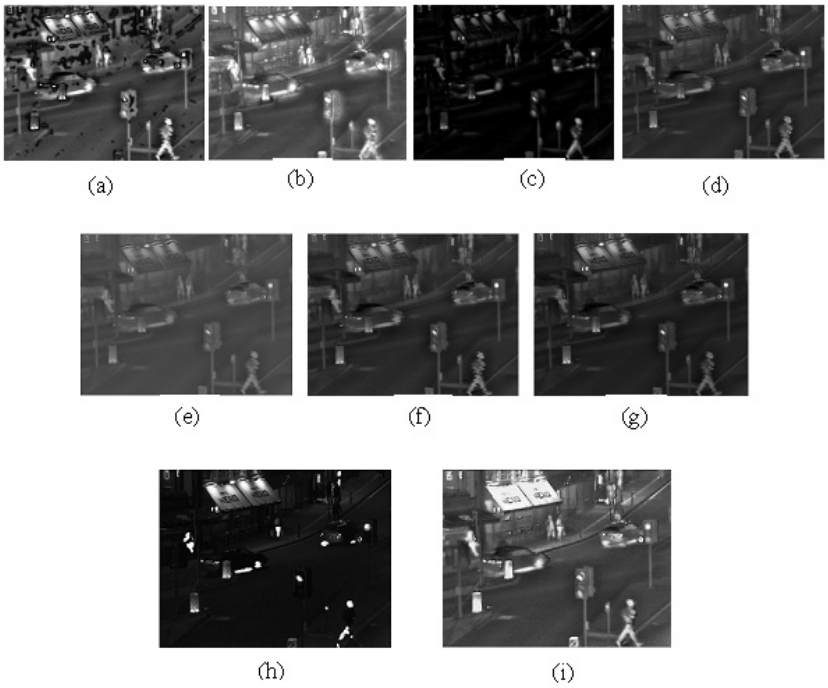

Fig. 7. Comparison of qualitative results of data set Image 3 (a) LP [6], (b) CP [7], (c) GF [10], (d) WSDCT [9], (e) DCDWT [42], (f) AD [11], (g) PCADWT [43], (h) FD [29], (i) Proposed.

Table 3. Quantitative metrics of data set Image 3.

Method / Metric	*MPI*	*SD*	*E*	*FS*	*AG*	*SF*	*VIF*
LP	11.745	20.087	4.825	0.09	1.704	4.274	0.277
CP	98.532	39.265	6.776	0.08	2.998	7.401	0.474
GF	72.850	38.423	6.928	0.166	5.07	13.379	**0.536**
WSDCT	51.834	21.039	5.928	0.096	3.130	9.162	0.349
DCDWT	51.532	21.346	5.964	0.078	2.806	9.142	0.277
AD	51.911	20.891	5.617	0.106	2.692	7.560	0.358
PCADWT	45.863	20.479	5.703	0.093	2.268	7.022	0.301
FD	25.287	34.525	5.167	0.133	3.029	15.791	0.146
Proposed	**126.989**	**49.957**	**7.220**	**0.06**	**13.909**	**36.085**	0.291

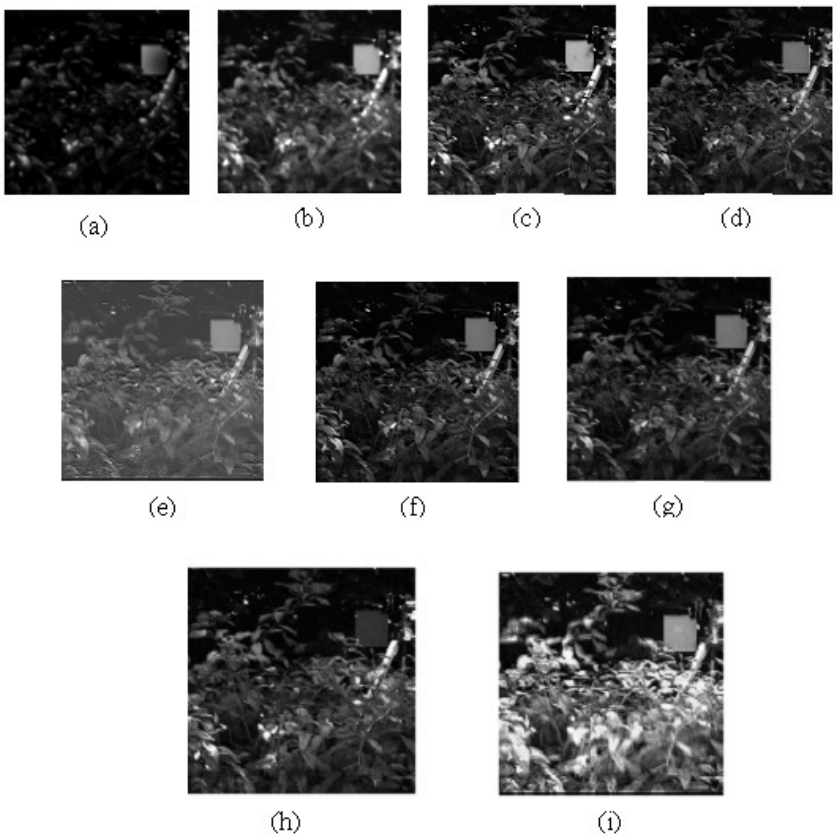

Fig. 8. Comparison of qualitative results of data set Image 4 (a) LP [6], (b) CP [7], (c) GF [10], (d) WSDCT [9], (e) DCDWT [42], (f) AD [11], (g) PCADWT [43], (h) FD [29], (i) Proposed.

Table 4. Quantitative metrics of data set Image 4.

Method / Metric	*MPI*	*SD*	*E*	*FS*	*AG*	*SF*	*VIF*
LP	15.088	22.124	5.209	**0.009**	3.085	6.969	0.311
CP	54.381	42.58	6.949	0.023	5.429	11.359	0.676
GF	44.604	42.251	6.753	0.06	9.593	21.521	0.859
WSDCT	35.463	31.573	6.4402	0.031	8.063	17.575	0.589
DCDWT	35.111	31.359	6.492	0.023	8.732	18.693	0.419
AD	35.518	31.34	6.396	0.031	7.100	15.516	0.603
PCADWT	35.959	31.327	6.411	0.032	7.138	15.578	0.610
FD	43.705	38.529	6.715	0.085	9.446	21.528	0.734
Proposed	**87.822**	**67.511**	**7.691**	0.025	**21.493**	**43.794**	**1.011**

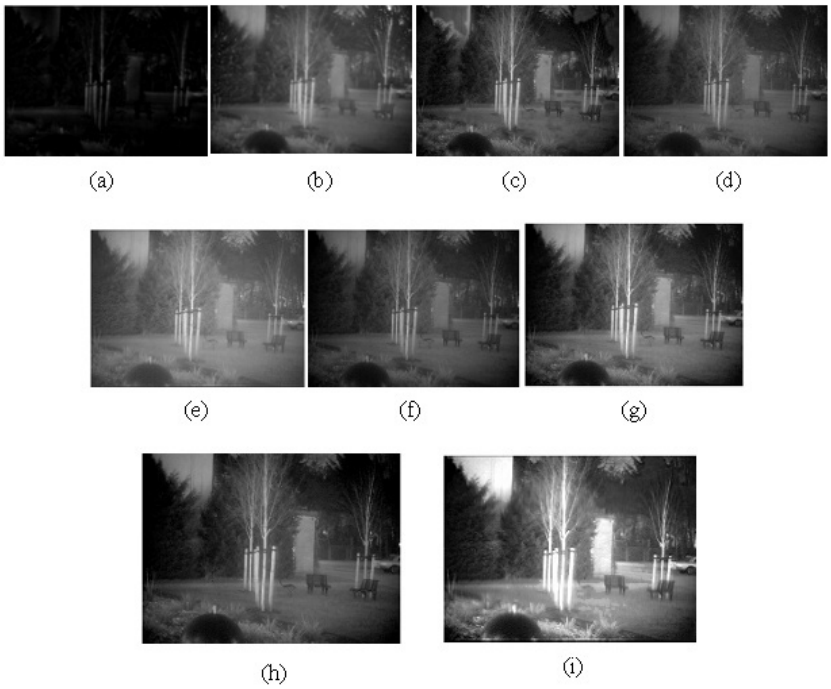

Fig. 9. Comparison of qualitative results of data set Image 5 (a) LP [6], (b) CP [7], (c) GF [10], (d) WSDCT [9], (e) DCDWT [42], (f) AD [11], (g) PCADWT [43], (h) FD [29], (i) Proposed.

The quantitative indices of the proposed work are shown in Tables 1-6. The quantitative metrics considered are the metrics that are frequently used in literature to assess the fusion algorithm. Therefore, the calculated metrics for the proposed method are compared with the values calculated by the state-of-art methods in literature. The metrics are computed for the data set images of various sizes without any normalisation. High MPI and SD values of the proposed work to all dataset images indicate high contrast in the final fused image. The information contained in both the source images are amassed with good clarity and sharpness that is being shown by the high AG value for all the data set images. High visual quality that demands the situational awareness of the scene is shown by high SF in all the simulated results.

Table 5. Quantitative metrics of data set Image 5.

Method / Metric	*MPI*	*SD*	*E*	*FS*	*AG*	*SF*	*VIF*
LP	7.297	9.802	4.331	0.088	1.311	2.985	0.198
CP	74.746	31.827	6.988	0.054	2.201	4.630	0.579
GF	59.743	34.988	7.032	**0.011**	4.674	9.120	0.844
WSDCT	58.956	29.629	6.862	0.054	3.556	6.740	0.473
DCDWT	58.430	29.866	6.868	0.072	3.501	6.948	0.453
AD	58.945	29.652	6.861	0.042	3.223	6.269	0.517
PCADWT	58.936	33.30	6.992	0.043	3.549	7.081	0.672
FD	59.079	39.338	7.081	0.096	4.506	9.125	0.882
Proposed	**97.858**	**59.199**	**7.695**	0.026	**7.379**	**15.878**	**1.347**

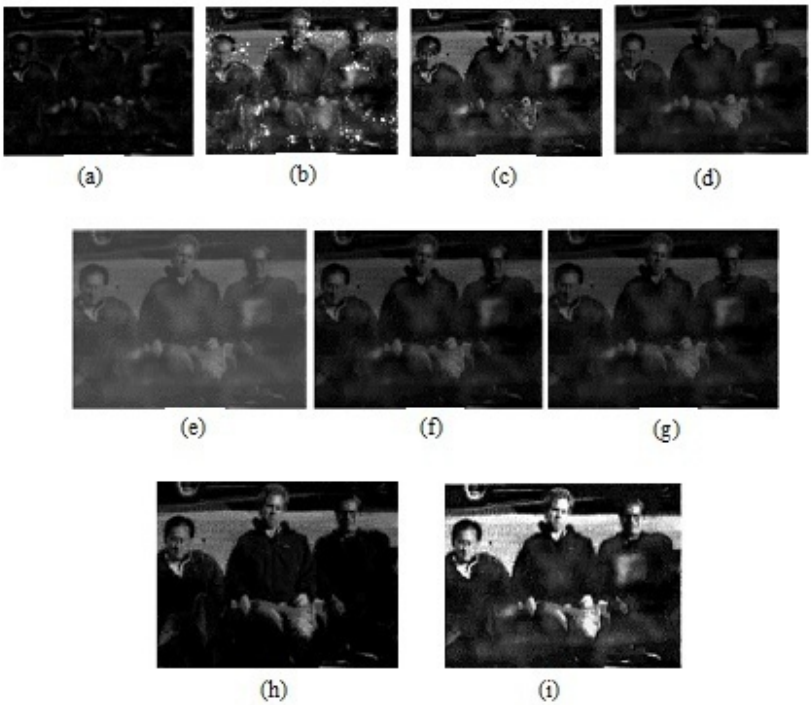

Fig. 10. Comparison of qualitative results of data set Image 6 (a) LP [6], (b) CP [7], (c) GF [10], (d) WSDCT [9], (e) DCDWT [42], (f) AD [11], (g) PCADWT [43], (h) FD [29], (i) Proposed.

Table 6. Quantitative metrics of data set Image 6.

Method / Metric	*MPI*	*SD*	*E*	*FS*	*AG*	*SF*	*VIF*
LP	11.533	17.278	4.938	0.286	2.131	6.220	0.179
CP	57.723	45.463	7.151	0.213	5.263	12.96	0.594
GF	42.907	38.421	6.767	**0.132**	5.666	14.665	0.532
WSDCT	26.63	25.907	6.121	0.223	3.764	11.056	0.342
DCDWT	25.995	23.182	6.089	0.250	4.508	14.691	0.266
AD	26.692	25.807	6.121	0.142	3.244	10.082	0.345
PCADWT	26.774	25.454	6.122	0.142	3.239	10.081	0.336
FD	25.847	43.305	5.034	0.163	3.669	15.241	0.348
Proposed	**61.599**	**67.876**	**7.174**	0.214	**8.423**	**21.976**	**0.851**

Table 7. Mean quantitative metrics over 6 data set images.

Method / Metric	*Contrast Metrics*		*Edge & Information Metrics*			**Visual Metrics**	
	MPI	**SD**	**AG**	**FS**	**E**	**SF**	**VIF**
LP	12.23	18.005	2.018	0.093	4.957	4.678	0.197
CP	86.83	37.8445	3.551	0.072	6.875	7.786	0.47
GF	68.09	37.37	6.82	0.074	6.89	14.57	0.5401
WSDCT	58.15	24.06	5.319	0.079	6.29	11.328	0.385
DCDWT	57.46	24.103	5.182	0.081	6.33	12.134	0.304
AD	58.20	23.86	4.555	0.065	6.27	9.756	0.398
PCADWT	57.38	27.04	4.797	**0.063**	6.402	10.305	0.406
FD	54.39	39.39	6.055	0.105	6.387	15.496	0.434
Proposed	**95.61**	**52.92**	**9.238**	0.066	**7.183**	**20.674**	**0.705**

Though the fusion symmetry is high for GF method, consistency in not maintaining large value to all images is observed. The same is the case observed for entropy and VIF metrics as shown in Tables 1-6. The mean quantitative metrics for the data set images are calculated and tabulated in Table 7. Summarizing the quantitative metrics it is observed that the proposed method provides highest mean contrast metrics MPI (95.61) and SD (52.92) that provide excellent overall contrast of the image. Average values of AG (9.238) and E (7.183) is observed to be high for the proposed method while the FS value of the proposed and PCADWT are comparable (0.066 & 0.063 respectively). This indicates that the proposed method provides excellent edge clarity and sharpness with good edge symmetry. Most of the information from the source images is preserved in the final image. The mean visual based metrics SF and VIF for CP, GF, WSDCT, DCDWT, AD, PCADWT and FD are high but the mean values (20.674 and 0.705 respectively) of the proposed method are largest indication better visual information of the captured scene for better interpretation and analysis. Comparative analysis proves that the proposed method enhances the contrast, preserves the edge information and provides the complete information of the complementary images in the amassed image.

5. Conclusion and Future scope:

A simple and novel fusion algorithm in spatial domain useful in military, defence and surveillance applications is proposed in this paper. The main aim of this paper is to provide the information from both the source images with clarity and with high contrast in a single image. The proposed adaptive window-based FD estimation provides an efficient edge, smooth and rough region feature extraction. The weight maps based on the estimated LFD of the proposed work reduces the computational complexity of weighted average fusion method. Enhancement of the low light visible image using lower and higher parameter based SR prior to the proposed fusion algorithm provides high contrast in the final fused image. Experimental evaluation and comparison with several existing algorithms is carried out that showed superior performance of the proposed method suitable for better scene interpretation. Feature extraction based fusion rules reduces artefacts and noise in the merged images compared to pixel level fusion rule. Feature- oriented level fusion improves the contrast of the fused image. Hence, our future work concentrates on the development of better feature extraction mechanism and enhancement based fusion algorithms for further improvement in the quantitative and qualitative results.

Nomenclatures

P_A	Marginal distribution of source image A.
P_{AF}	Joint probability distribution between source image A and fused image F.
P_B	Marginal distribution of source image B.
P_{BF}	Joint probability distribution between source image B and fused image F.
P_F	Marginal distribution of fused image F.

Abbreviations

AD	Anisotropic Diffusion

CP	Contrast Pyramid
DWT	Discrete Wavelet Transform
FD	Fractal Dimension
GF	Guided Filtering
LFD	Local Fractal Dimension
LP	Laplacian Pyramid
SR	Stochastic Resonance
SVD	Singular Value Decomposition

References

1. Toet,A.; IJspeert,J.K.; Waxman,A.M.; and Aguilar,M. (1997). Fusion of visible and thermal imagery for situational awareness. *Displays*,Proceedings SPIE,3088,85-95.
2. Das,S.;Zhang,Y.L.; and Krebs,W.K.(2000). Color night vision for navigation and surveillance.*Proceedings of the Fifth Joint Conference on Information Sciences,* Atlantic City, NJ.
3. Bhatnagar,G.; and Liu,Z. (2015). A novel image fusion framework for night-vision navigation and surveillance. *Signal, Image and Video Processing*, 9, 165-175.
4. Chavez,P.S.; andKwarteng,A.Y. (1989).Extracting spectral contrast in landsat thematic mapper image data using selective principal component analysis.*Journal on Photogram. Engineering Remote Sensing*, 55(3), 339-348.
5. Shutao Li; James T. Kwok; and Yaonan Wang. (2001). Combination of images with diverse focuses using the spatial frequency. *Information Fusion*, Elsevier Publishers, 2(3), 169-176.
6. Peter Burt,J.; and Edward Adelson,H.(1983). The laplacian pyramid as a compact Image Code, *IEEE Transactions on Communications*, 31(4), 532-540.
7. Toet,A.(1989).Image fusion by a ratio of low pass pyramid. *Pattern Recognition Letters*,9(4),245 -253.
8. Li,H.; Manjunath,B.S.;andMitra,S.K. (1995). Multisensor image fusion using the wavelet transform. *Graphical Models and Image Processing*, Elsevier Publications, 57(3), 235-245.
9. Naidu,V.P.S. (2018). Block DCT based image fusion techniques. Retrieved February 18,2018, from http://e-jst.teiath.gr.
10. ShutaoLi.; Xudong Kang; andJianwen Hu. (2013).Image fusion with guided filtering.*IEEE Transactions on Image processing*, 22(7), 2864-2875.
11. DurgaPrasad,B.; and Ravindra Dhuli. (2015). Fusion of infrared and visible sensor images based on anisotropic diffusion and Karhunen-Loeve transform. *IEEE Sensors Journal*,16(1),203-209.
12. Shoulin Yin; and Ye Zhang. (2019). Singular value decomposition-based anisotropic diffusion for fusion of infrared and visible images. *International Journal of Image and data fusion*, 10(2), 146-163.
13. Gaurav Bhatnagar; and Zjeng Li. (2017). Multi-sensor fusion based on local activity measure. *IEEE Sensors Journal*,17(22),7487-7496.

14. Weiling Yin; Wenda Zhao; Di You; and Dong Wang. (2019). Local binary pattern metric-based multi-focus image fusion. *Optics and Laser Technology*, 110, 62-68.
15. JiayiMa; Yong Ma; and Chang Li. (2019). Infrared and visible image fusion methods and applications: A survey. *Information Fusion*, 45, 153-178.
16. Huang,Q.; Ye,H.; He,X.; and Zhang,C. (2004). Image enhancement using stochastic resonance. *In International Conference on Image Processing*, 263-266.
17. Rallabandi,V.P.S.(2008). Enhancement of ultrasound images using stochastic resonance-based wavelet transform. *Computerized Medical Imaging and Graphics*, 32(4), 316-320.
18. Rallabandi,V.P.S; and Roy,P.K. (2010). Magnetic resonance image enhancement using stochastic resonance in Fourier domain. *Elsevier Publications on Magnetic Resonance Imaging*,28(9), 1361-1373,
19. Gonzalez,R.C.; and Woods,E. (2014).*Digital Image Processing*(4th ed.). Pearson Publications.
20. Yeong-Taeg Kim. (1997). Contrast enhancement using brightness preserving bi-histogram equalization. *IEEE Transactions on Consumer Electronics*, 43(1), 1-8.
21. Yu Wang; Qian Chen; and BaeominZhang. (1999). Image enhancement based on equal area dualistic sub-image histogram equalization method. *IEEE Transactions on Consumer Electronics*, 45(1), 68-75.
22. Wharton Eric,J.; Panetta Karen,A.; and AgaianSos,S. (2007). Human visual system based image enhancement. *In Proceedings of SPIE Defense and Commercial Sensing*,6579.
23. Chouhan,R.; Jha,R.K.; and Biswas, P.K. (2013). Enhancement of dark and low-contrast images using dynamic stochastic resonance. *IET Image Processing*, 7(2), 174-184.
24. Sandhya KumariTeku; KoteswaraRao,S.; and Santi Prabha,I. (2016). Contrast enhanced low-light visible and infrared image fusion.*Defence Science Journal*, 66(3), 266-271.
25. Chouhan,R.; Biswas,P.K.; and Jha,R.K. (2015). Enhancement of low- contrast images by internal noise-induced Fourier coefficient rooting.*Signal, Image and Video Processing Journal*,Springer Publications, 9, 255-263.
26. Dawen Huang; Jianhua Yang; Jingling Zhang; and Houguang Liu. (2018).An improved adaptive stochastic resonance with general scale transformation to extract high-frequency characteristics in strong noise. *International Journal of Modern Physics*,32(15).
27. Hind Taud et Jean-Francios Parrot.(2005).*Geomorphologie: relief, processus,environnement*,11(4), 327-338.
28. Toennies,K.D.; and Schnabel,J.A. (1994).Edge detection using the local fractal dimension.*Proceedings of IEEE Symposium on Computer-Based Medical Systems*, Winston-Salem, NC, USA, 34-39.
29. Gaurav Bhatnagar; and Wu,Q.M.J. (2019). A Fractal dimension based framework for night vision fusion. *IEEE/CAA Journal of AutomaticaSinica*, 6(1), 220-227.

30. SonnyNoviznto; YukinoriSuzuki; and Junji Maeda.(2002).Optimum estimation of local fractal dimension based on the blanket method.*IPRJ Journal*, 43(3).
31. Mehdi Roopaei; SosAgaian; Mehdi Shadaram; and Frank Hurtado. (2014). Cross-entropy histogram equalization. *IEEE International Conference on Systems, Man, and Cybernetics,* San Diego, CA, 158-163
32. Agaiani,S.; Roopaei,M.; Shadaram,M.; and Bagalkot,S.S. (2014). Bright and dark distance-based image decomposition and enhancement. *IEEE International Conference on Imaging systems and techniques Proceedings*, Santorini, 73-78.
33. Jha,R.K.; and Chouhan,R. (2014). Noise-induced contrast enhancement using stochastic resonance on singular values. *Signal, Image & Video Processing*, 8, 339-347.
34. Michael Braukus; and Keith Henry. (2001). Retrieved March 20, 2018, from http://dragon.larc.nasa.gov/retinex/pao/news/
35. Peleg,S.; Naor,J.; Hartley,R; and Avnir,D. (1984). Multiple resolution texture analysis and classification. *IEEE Transactions on Pattern Analysis and Machine intelligence*, 6(4), 518-523
36. Chen Feng; Guangrong Ji; Junna Cheng; Xuefeng Liu; and Jie Zhang. (2008).Image edge detection based on improved local fractal dimension.*Fourth International Conference on Natural Computation*, Jinan, 640-643.
37. RichardVuduc. (1997).Image segmentation using fractal dimension. *GEOL 634*, CornellUniversity.
38. Ravinandan,M.E.; and Jharna Majumdar.Feature based image fusion. *Proceedings of the International Conference on Cognition and Recognition*, 958-964.
39. Yu Han; Yunze Cai; Yin Cao; and Xiaoming Xu. (2013). A new image fusion performance metric based on visual information fidelity. *Information Fusion*, 14(2), 127-135.
40. Toet,Alexander. (2014). Retrieved April 26, 2014, from https://figshare.com/articles/TNO_Image_Fusion_Dataset/1008029
41. Xiang Yan; Hanlin Qin; Jia Li; Huixin Zhou; and Jing-Guo Zong. (2015). Retrieved September 11, 2015, from http://home.ustc.edu.cn/liuvu1/
42. Tian Pu.; and GuoqiangNi. (2000). Contrast-based image fusion using the discrete wavelet transform. *Journal of Optical Engineering*, 39(8), 2075-2082.
43. Vijayarajan,R.; and Muttan,S. (2015). Discrete wavelet transform based principal component averaging fusion for medical images. AEU-*International Journal of Electronics and Communications*, 69(6), 896-902.